
SPATIO-TEMPORAL JOINT MODELLING ON MODERATE-EXTREME AIR POLLUTION IN SPAIN

Kai Wang

Wisdom Lake Academy of Pharmacy
Xi'an Jiaotong-Liverpool University
Kai.Wang17@student.xjtlu.edu.cn

Chengxiu Ling

Wisdom Lake Academy of Pharmacy
Xi'an Jiaotong-Liverpool University
Chengxiu.Ling@xjtlu.edu.cn

Ying Chen

Wisdom Lake Academy of Pharmacy
Xi'an Jiaotong-Liverpool University
Ying.Chen01@student.xjtlu.edu.cn

Zhengjun Zhang

Department of Statistics
University of Wisconsin-Madison
zjz@stat.wisc.edu

ABSTRACT

Extremely poor air quality is consistently connected with numerous diseases. Appropriate extreme analysis and accurate predictions are in rising demand for exploring potential linked causes and for providing suggestions for the environmental agency in public policy strategy. This paper aims to model the spatial and temporal pattern of both moderate and extremely poor PM_{10} concentrations (of daily mean) collected from 342 representative monitors distributed throughout mainland Spain from 2017 to 2021. We firstly propose and compare a series of Bayesian hierarchical generalized extreme models of annual maxima PM_{10} concentrations, including both the fixed effect of altitude, temperature, precipitation, vapour pressure and population density, as well as the spatio-temporal random effect with the Stochastic Partial Differential Equation (SPDE) approach and a lag-one dynamic auto-regressive component (AR(1)). The similar and different effects of interrelated factors are identified through a joint Bayesian model of annual mean and annual maxima PM_{10} concentrations, which may bring the power of statistical inference of body data to the tail analysis with implementation in the faster and more accurate Integrated Nested Laplace Approximation (INLA) algorithm with respect to MCMC. Under WAIC, DIC and other criteria, the best model is selected with good predictive ability based on the first four-year data (2017-2020) for training and the last-year data (2021) for testing. The findings are applied to identify the hot-spot regions with extremely poor quality using excursion functions specified at the grid level. It suggests that the community of Madrid and the northwestern boundary of Spain are likely to be exposed to severe air pollution simultaneously exceeding the warning risk threshold. The joint model also provides evidence that certain predictors (precipitation, vapour pressure and population density) influence comparably while the other predictors (altitude and temperature) impact oppositely in the different scaled PM_{10} concentrations.

Keywords Extreme Value Analysis · Air Pollution · Bayesian Joint model with sharing effects · Spatio-temporal model · Integrated Nested Laplace Approximation

1 2

¹This project is supported by the Research Development Fund at XJTLU (RDF1912017), the Post-graduate Research Scholarship (PGRS2112022) and Jiangsu Qinglan Talent in 2022.

²Corresponding author: Chengxiu Ling, email: Chengxiu.Ling@xjtlu.edu.cn

1 Introduction

Air pollution, composed of particulate matter (PM) and gaseous pollutants, has a substantial negative impact on the environment, ecosystem and human health. Poor air quality is one of the five most significant health risks worldwide, alongside high blood pressure, smoking, diabetes and obesity (Cohen et al., 2017; Daellenbach et al., 2020). It becomes one of the most considerable health concerns for the residents in areas of higher population density (Dias and Tchepel, 2018), centres with dense activities, and to particular user groups (Agarwal and Kaddoura, 2019; Singh et al., 2021). Among all the pollutants, the particulate matter, with an aerodynamic diameter less than or equal to 10 and 2.5 microns respectively (PM₁₀ and PM_{2.5}) are most consistently connected with numerous adverse health outcomes including lung infections, cardiovascular diseases, and respiratory problems (Joseph et al., 2003; Martuzzi et al., 2006; Samoli et al., 2013).

In Europe, although the European Environment Agency (EEA) maintains a rather dense particulate matter monitoring network to record the concentration levels across countries, huge regions of the European continent remain unmonitored. For proper assessment of population-wide exposure and appropriate formulation of pollution mitigation strategies, the responsible authorities need accurately estimated and predicted concentration levels at the unobserved locations (Chu et al., 2015).

The main challenge to the forecast of particulate matter concentrations corresponds to the complexity of PM generation and spreading dynamics. On the one hand, the PM generation is dominated by two complicated sources, inorganic aerosol coming from the agriculture, long-range transport and energy sectors (Daellenbach et al., 2020), as well as organic aerosol coming from biomass and fossil fuels burning emissions, vehicles emissions and cooking (Lenschow et al., 2001; Omidvarborna et al., 2015). On the other hand, the PM spread depends on both meteorological conditions and land use dispersion, leading the observed concentration levels to fluctuate geographically and temporally.

In the statistical literature, the Bayesian spatio-temporal model that allows modelling a complex environmental phenomenon through a hierarchy of sub-models becomes one of the most promising methodologies in air quality scientific investigations (Cameletti et al., 2013; Amin et al., 2015; Taheri Shahraiyni and Sodoudi, 2016; Forlani et al., 2020; Fioravanti et al., 2021; Castro-Camilo et al., 2021). In particular, this approach allows to involve the explanatory variables to explain the large-scale variability, take residual dependency into account through a space-time process with a Gaussian Random Field (GRF), and produce high-resolution spatial forecasts to meet the rising demand for predictive concentration maps in epidemiological studies.

According to Porcu et al. (2012), the main drawback of the Bayesian model with a Gaussian Random Field (GRF) refers to the computational difficulty to deal with enormous amounts of data, especially applying complex spatial dependence measures (i.e., the Matérn covariance function). Some strategies have been proposed to alleviate the computational burden of fitting complex spatial and temporal models. Lindgren et al. (2011) proposed the Stochastic Partial Differential Equation (SPDE) approach, providing a method to represent a continuous Matérn field through a discretely indexed Gaussian Markov random field (GMRF) associated with a sparse precision matrix, which enjoys good computational property. Rue et al. (2009) also provided the Integrated Nested Laplace Approximation (INLA) algorithm that performs direct numerical calculations on the marginal posterior distributions, avoiding the time-consuming Markov chain Monte Carlo (MCMC) simulations. Additionally, GMRF with SPDE approach can be fitted in a Bayesian hierarchical framework through the INLA approach, with implementation in the R-INLA package available at <https://www.r-inla.org/>, making this methodology fast and easily implemented.

Most previous spatial and temporal studies on air pollution only concentrated on moderate PM concentrations (Sahu, 2012; Cameletti et al., 2013; Beloconi et al., 2018; Fioravanti et al., 2021). However, extreme conditions are actually more concerned with environmental quality management due to their various hazardous impacts (Amin et al., 2015). Especially, numerous epidemiological studies pointed out that short-term exposures to severe particulate matter pollution can trigger serious acute cardiovascular events (Mustafić et al., 2012; Yu et al., 2014; Brook et al., 2016) and huge economic loss in the corresponding hospitalization (Shah et al., 2013). In the field of extreme case spatio-temporal analysis, Sharma et al. (2012); Amin et al. (2015); Martins et al. (2017) and Castro-Camilo et al. (2021) typically focused on a small spatial domain, making it difficult to consider the complicated orography with a variety of climatic conditions, as well as to provide general suggestions to national governments on the environmental policy formulation and health care allocation. More importantly, to our best knowledge, no studies consider the potential difference between moderate and extreme air pollution, in other words, model different scaled air pollution simultaneously to identify similarities and differences in the effects of influential factors.

In this paper, we focus on the spatial and temporal variation of both moderate and extreme air pollution in Spain, in particular, annual mean and annual maxima of daily PM₁₀ concentration levels from 2017 to 2021. Firstly, we establish several Bayesian hierarchical generalized extreme models on annual maxima and compare their predictive performance under specific criteria on both training and validation sets. Moreover, we generate the excursion function

maps (Bolin and Lindgren, 2015) based on the best model selected in the previous phase, aiming to highlight the regional risk ranking that simultaneously exceeds the warning risk threshold, see details in Sections 3.2, 4.1 and 4.3. Secondly, we identify and analyse the similar and different effects of predictors in Sections 3.3 and 4.4 to annual mean and maxima concentrations by the joint Bayesian model with sharing effects, the result of which suggests the comparable influence of precipitation, vapour pressure and population density as well as the opposite effects of altitude and temperature. The main findings with high-resolution spatial forecasts and comprehensive knowledge on the PM₁₀ generation and spread are expected to promote awareness of the significance of extreme air pollution research, help in the investigation of the long-term effect in epidemiological studies, and serve as a reference for environmental agencies in air pollutants regulation and human health protection.

The rest of the paper is organized as follows. In Section 2 we demonstrate the dataset for response and main explanatory variables. In Section 3 we formalize spatio-temporal Bayesian generalized extreme models on moderate-extreme air pollution in the framework of Bayesian spatial analysis and extreme value theory. We present main results, applications and potential influence in Section 4, and conclude this paper with extensional discussions in Section 5.

2 Data

2.1 PM₁₀ concentrations and spatial domain

In mainland Spain, the PM₁₀ concentration levels data is accessible by the Air Quality e-Reporting which is EEA's air quality database consisting of a multi-annual time series data of air quality measurement and calculated statistics for a number of air pollutants. To work with a more robust dataset, we only retain 342 air pollution stations that have at least 60% valid observations in a year, with the geographical distribution of the stations shown in red circles embedded in the mesh constructed for SPDE approach (Figure 1). This five-year dataset (2017-2021) with 1470 observations is divided into the training set (2017-2020; 1215 observations) and the validation set (2021; 255 observations), which are used to evaluate and compare the model fitness and predictive ability.

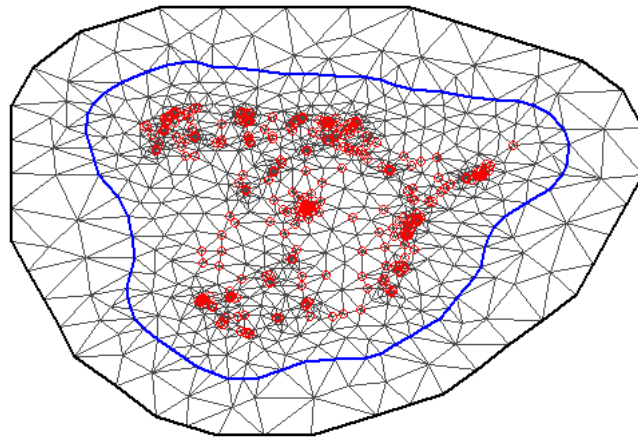


Figure 1: Study domain together with the spatial distribution of the 342 monitoring sites in red circles. The figure also illustrates the mesh used to build the SPDE approximation to the continuous Matérn field.

The temporal and spatial variations of extreme PM₁₀ pollution are shown in detail in Figure 2. Temporally, severe pollution seems to occur in 2017 and 2020, as indicated by the numerous monitors coloured in red (very poor) and purple (extremely poor). Spatially, compared with relatively low annual maxima recorded in the east (Valencian Community) and north (Basque Country), high PM₁₀ concentrations are most prevalent in the centre, northwest, and southeast, which correspond to the autonomous communities of Madrid, Galicia, Andalusia, and the Region of Murcia, respectively. This spatio-temporal pattern inspires our further investigation of spatio-temporal modelling taking appropriate topography covariates into account, which are stated in the following section.

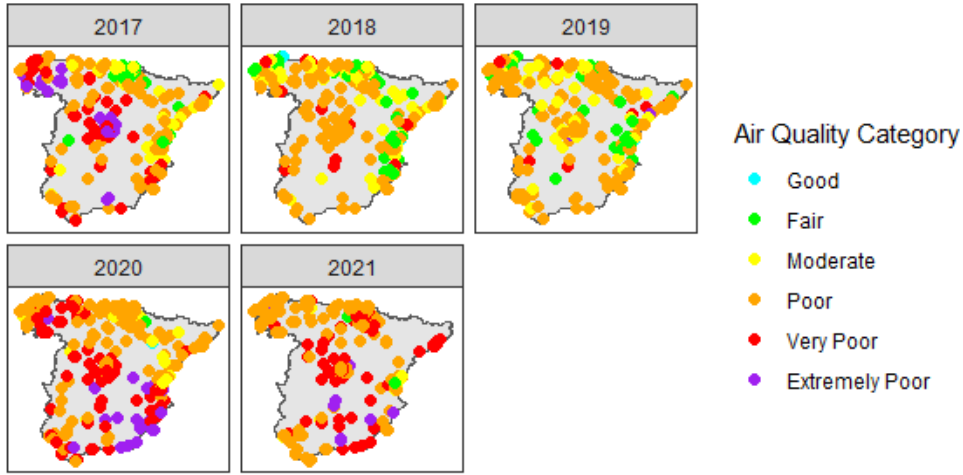


Figure 2: Spatio-temporal patterns of annual maxima PM_{10} concentration levels in Year 2017–2021 throughout mainland Spain. The annual data is reported by European Environment Agency (EEA) and shown in the heat map with EEA's air quality category.

Table 1: Description for explanatory variables.

Predictors	Description	Units	Spatial Resolution
Altitude	Altitude of PM_{10} monitors	m	Station Specific
Temperature	Annual mean temperature	°C	50km × 50km
Precipitation	Annual mean precipitation	mm/month	50km × 50km
Vapour Pressure	Annual mean vapour pressure	hPa	50km × 50km
Population Density	Number of people per unit area	per km ²	Autonomous Communities

2.2 Explanatory variables

A number of potential predictors are available based on prior findings in the air quality literature (Cameletti et al., 2013; Fioravanti et al., 2021; Castro-Camilo et al., 2021)), and we choose to include a set of five main spatial and spatio-temporal varying predictors with the complete description list reported in Table 1.

In the following, we describe the selected predictors more in details.

Meteorological variables. The meteorological variables (temperature, precipitation and vapour pressure) of monthly mean are collected from the CRU TS (Climatic Research Unit gridded Time Series; Harris et al., 2020) dataset and aggregated to be annual mean. Accordingly, CRU TS was first published in 2000, using ADW (angular-distance weighting) to interpolate anomalies of monthly observations onto a 0.5° grid over land surfaces (excluding Antarctica) for observed and derived variables (mean, minimum and maximum temperatures, precipitation, vapour pressure, wet days and cloud cover) with no missing values in the defined domain.

Elevation. The altitude data, height over sea level, matched with locations of all air pollution monitors, is accessible in the annual aggregated air quality values dataset provided by EEA, available at <https://discomap.eea.europa.eu/App/AirQualityStatistics/index.html>.

Population Density. The population densities are calculated in each autonomous communities. The original data is collected from statistics report (available at <https://stats.oecd.org/>) of the Organisation for Economic Co-operation and Development (OECD). The OECD statistics contains data and metadata for economic and education indexes of OECD countries and some selected non-member economies.

We see in Table 2 that the correlations of potential predictors to extreme and average PM_{10} display a similar or different direction, which also vary year by year. This will be further investigated by our spatio-temporal generalized extreme model and joint model with sharing effects, see details in both Sections 3.2 and 3.3. Furthermore, considering some

significant connections between location variables and meteorological variables (e.g., latitude and temperature), and we adjust the location variables (longitude and latitude) as covariates in our models below.

Table 2: Correlation between explanatory variables and annual mean and annual maximum PM₁₀ on log scale.

Explanatory variables	Correlation to ln mean (ln max) in years (sample size)					
	2017 (294)	2018 (296)	2019 (300)	2020 (325)	2021 (255)	Total (1470)
Altitude	-0.34 (0.39)	-0.39 (0.39)	-0.40 (0.13)	-0.31 (-0.24)	-0.24 (-0.01)	-0.34 (0.32)
Temperature	0.28 (-0.02)	0.28 (0.01)	0.34 (0.15)	0.31 (0.19)	0.33 (-0.13)	0.30 (0.08)
Precipitation	-0.13 (-0.19)	-0.08 (-0.15)	-0.14 (0.01)	-0.21 (-0.27)	-0.25 (-0.13)	-0.18 (-0.20)
Vapour Pressure	0.28 (-0.15)	0.33 (-0.05)	0.36 (0.17)	0.32 (0.23)	0.29 (-0.25)	0.31 (0.02)
Population Density	0.06 (0.28)	0.04 (0.09)	0.02 (0.02)	0.01 (0.02)	-0.01 (0.11)	-0.02 (0.10)

3 Model Formulation

In this section, we first introduce the main methodology involved in spatio-temporal Gaussian field and extreme value models in Section 3.1. This will be utilized in Section 3.2 to establish four candidated models of annual maximum of daily PM₁₀ in mainland Spain. Finally, we propose a joint Bayesian Gumbel-Gaussian model for extreme and moderate PM₁₀ in Section 3.3.

3.1 Spatial and temporal models

In this section, we introduce two typical approaches to respectively measure spatial and temporal dependence that can not be explained by the covariates: Matérn covariance function with SPDE approximation for spatial correlation and the auto-regressive (AR) dynamic model for temporal dependence. Meanwhile, the generalized extreme value model is recalled to investigate the extreme poor air quality (annual maximum of daily PM₁₀) behavior.

Matérn covariance function and SPDE approach. The Matérn covariance function, also known as Matérn kernel (Genton, 2002), is widely applied in spatial statistics, geostatistics, machine learning and image analysis due to its flexible local behaviour and attractive theoretical properties (Matérn, 1986; Guttorp and Gneiting, 2006). It is commonly used to evaluate the statistical covariance between two locations, while the covariance only depends on the distance and becomes isotropic for the Euclidean measure. Given the spatial correlated effects $w(s_i)$ and $w(s_j)$ at two locations s_i and s_j separated by $d(s_i, s_j)$ units, the Matérn covariance function is in the form of

$$\text{Cov}(w(s_i), w(s_j)) = \frac{\sigma^2}{2^{\nu-1}\Gamma(\nu)} \left(\sqrt{8\nu} \frac{d(s_i, s_j)}{\rho} \right)^\nu K_\nu \left(\sqrt{8\nu} \frac{d(s_i, s_j)}{\rho} \right), \quad (1)$$

where $w(s), s \in \mathcal{S}$ is a random field, and $d(s_i, s_j)$ is normally the Euclidean distance, Γ is the gamma function, K_ν is the modified Bessel function of the second kind, $\rho > 0$ is the range parameter, $\nu > 0$ is the smoothness parameter, and $\sigma > 0$ for the marginal variance. The application of the Matérn covariance function in the latent Gaussian model rapidly increases after the proposal of the Stochastic Partial Differential Equations approach (SPDE; Lindgren et al., 2011). Given a continuous Matérn field defined on the domain in two-dimensional space (i.e., a second-order stationary and isotropic Gaussian Field $w(s)$, $s \in \mathcal{S} \subset \mathbb{R}^2$ with a Matérn covariance function defined in Eq.(1), denoted by $w(s) \sim \mathcal{GP}_{2D-SPDE}(\rho, \sigma, \nu)$), the SPDE approach basically uses a finite element representation to define the continuous Matérn field as a linear combination of basis functions defined on a triangulation of the domain. This representation makes it possible to use a Gaussian Markov random field (GMRF) as the best representative of the given Matérn field, while the GMRF with a local neighbourhood in a sparse precision matrix enjoys its good computational properties. This allows for avoiding the “big n problem” that arises when working with the dense covariance matrix of the Gaussian Field (Cameletti et al., 2013).

Auto-regressive model. The auto-regressive (AR) model is a linear predictive modelling technique (Gandhi, 2015). It relies on previous observations to predict current ones by using the AR parameters as coefficients. Specifically, the current period values are modelled by a sum of past outcomes multiplied by a numeric factor. For the inclusion of p number of lagged values, we denote the AR model as AR(p), where p is called the order of the model. As we concern with the annual maxima concentration, it is less likely that the auto-correlation phenomenon lasts for a few years, also, for simplicity, we use the AR(1) with Gaussian white noise when considering the temporal dependence in our context.

An AR(1) model is defined as follows (Shumway and Stoffer, 2011). Let $X_t, t \in \mathbb{N}$ be a stationary time series with mean zero, satisfying

$$X_t = aX_{t-1} + \varepsilon_t,$$

where ε_t 's is a white noise process with zero mean and constant variance. Here a is a numeric constant by which we multiply the lagged variable X_{t-1} , which is interpreted as the part of the previous value which remains in the present.

Generalized extreme value models. According to the Extremal Types Theorem introduced by Fisher and Tippett (1928a) and Coles (2001), both Generalised Extreme Value (GEV) and Gumbel distribution (that is, GEV with extreme value index equal zero) are appropriate to model extreme datasets e.g., air quality. The GEV distribution has three parameters, location parameter ($\mu, -\infty < \mu < \infty$), scale parameter ($\sigma, \sigma > 0$) and tail parameter ($\xi, -\infty < \xi < \infty$) with the cumulative distribution function

$$\text{GEV}(x; \mu, \sigma, \xi) = \exp \left\{ - \left[1 + \xi \left(\frac{x - \mu}{\sigma} \right) \right]^{-\frac{1}{\xi}} \right\},$$

defined on the set $\{x : 1 + \xi(x - \mu)/\sigma > 0\}$. The case $\xi = 0$ is interpreted as the limit of as $\xi \rightarrow 0$, leading to the Gumbel family with distribution function

$$\text{Gumbel}(x; \mu, \sigma) = \exp \left\{ - \exp \left[- \left(\frac{x - \mu}{\sigma} \right) \right] \right\}, \quad x \in \mathbb{R}.$$

3.2 Spatio-temporal extreme value models with mixed effects

With the spatial and temporal components introduced in Section 3.1, we establish two groups of generalised extreme value models with similar fixed effects and varying random effects to model the annual maxima PM_{10} concentrations.

Model 1: Gumbel model with fixed effect and spatio-temporal random effect. Let $y_{max}(s, t)$ denote the logarithm transform of annual maxima PM_{10} concentrations at location $s \in \mathcal{S}$ and year $t \in \mathcal{T}$, where \mathcal{S} is the study area and \mathcal{T} is the time period in focus. Under the assumption of constant scale (σ) and tail (ξ) parameters, we use a linear combination of fixed effects with explanatory variables and spatio-temporal varying random effect to model the location parameter ($\mu(s, t)$) in Gumbel model below. Suppose that

$$[y_{max}(s, t) \mid \mu(s, t), \sigma] \sim \text{Gumbel}(\mu(s, t), \sigma) \quad \text{with} \quad \mu(s, t) = \mathbf{x}(s, t)^\top \boldsymbol{\beta} + u(s, t) \quad (2)$$

and

$$\begin{aligned} u(s, t) &= au(s, t-1) + w(s, t), \\ w(s, t) &\sim \mathcal{GP}_{2D-SPDE}(\rho_M, \sigma_M, \nu_M). \end{aligned} \quad (3)$$

Here, the fixed effects are associated with the covariate vector $\mathbf{x}(s, t)$ including an intercept plus the explanatory variables of location variables, meteorological variables and human-effect variables listed in Table 1, and the vector $\boldsymbol{\beta}$ corresponds to the regression coefficients associated with the fixed effects, while $u(s, t)$ denotes a random effect that spatially changes with the Matérn covariance function and temporally follows the structure of AR(1) dynamics.

Model 2: Gumbel model with fixed effect and separated spatial and temporal random effect. Our second model is a modification of Model 1 specified in Eq.(2) with separate SPDE-spatial random effect and AR(1) model instead. That is, we keep the Gumbel distribution assumption on $y_{max}(s, t)$ with the same fixed effects. The spatio-temporal effect $u(s, t)$ is re-specified as

$$\begin{aligned} u(s, t) &= f(t) + w(s), \\ f(t) &\sim \mathcal{GP}_{\text{AR}(1)}(a, \tau_{AR}), \\ w(s) &\sim \mathcal{GP}_{2D-SPDE}(\rho_M, \sigma_M, \nu_M). \end{aligned} \quad (4)$$

Note that the $f(t)$ denotes the non-linear random effect in the temporal structure of AR(1) and the $w(s)$ is the spatially dependent only random effect with SPDE structure. Specifically, the implementation of the AR(1) model in INLA generally assumes the Gaussian white noise with mean 0 and precision τ_{AR} . For $f(t)$ defined over the naturally binned covariate (Year), let $\mathbf{t} = (t_1, \dots, t_5)^\top$ denotes the time from the first year (t_1) to the last year (t_5),

$$\begin{aligned} f(t_1) &\sim \mathcal{N}\left(0, (\tau_{AR}(1 - a^2))^{-1}\right), \\ f(t_i) &= af(t_{i-1}) + \epsilon_i, \quad \epsilon_i \sim \mathcal{N}(0, \tau_{AR}^{-1}), \quad i = 2, \dots, 5, \end{aligned}$$

where $-1 < a < 1$ is a numeric constant, the so-called auto-correlation, by which we multiply the lagged variable $f(t_{i-1})$, and ϵ_i denotes the unpredictable error in the form of Gaussian white noise.

Model 3: GEV model with fixed effect and spatio-temporal random effect. The generalised extreme value (GEV) models are basically following the same structure as Gumbel models except the generalized extreme value distribution for the response. To be specific, we suppose that

$$[y_{max}(\mathbf{s}, t) | \mu(\mathbf{s}, t)] \sim \text{GEV}(\mu(\mathbf{s}, t), \sigma, \xi), \quad (5)$$

where the location parameter $\mu(\mathbf{s}, t)$ is of the same form of mixed effects as in Eq.(2) and random effects in Eq. (3). Note that this model generalizes Gumbel model with spatio-temporal random effects, since the GEV model with $\xi = 0$ corresponds to the Gumbel model.

Model 4: GEV model with fixed effect and separated spatial and temporal random effect. Similar consideration of Model 2 modified from Model 1, we consider the following model in parallel with Model 3, i.e., we take separate spatial and temporal random effects into the GEV model. Suppose that

$$[y_{max}(\mathbf{s}, t) | \mu(\mathbf{s}, t), \sigma, \xi] \sim \text{GEV}(\mu(\mathbf{s}, t), \sigma, \xi) \quad (6)$$

with the location parameter $\mu(\mathbf{s}, t)$ is of spatio-temporal structure of the form in Eqs.(2) and (4).

3.3 Bayesian joint model with sharing effects

In order to identify the potential varied effect levels of main explanatory variables, with inspiration from applications of the joint model with sharing effects on wildfire (Joseph et al., 2019; Sevinc et al., 2020; Koh et al., 2021), we model both moderate and extreme PM_{10} pollution simultaneously in two respective sub-models linked by the sharing effects and the sharing coefficients (scaling factors).

Let $y_{mean}(\mathbf{s}, t)$ denote the logarithm transform of annual mean PM_{10} at location $\mathbf{s} \in \mathcal{S}$ and year $t \in \mathcal{T}$. We perform Gaussian sub-model and Gumbel sub-model on annual mean and annual maxima respectively, with the structure of the best extreme value model as Model 1 according to the model fitness and prediction analysed in Section 4.1.

$$\begin{aligned} [y_{mean}(\mathbf{s}, t) | \mu_{mean}(\mathbf{s}, t), \sigma_{mean}^2] &\sim \text{Gaussian}(\mu_{mean}(\mathbf{s}, t), \sigma_{mean}^2) \quad \text{with} \\ \mu_{mean}(\mathbf{s}, t) &= \mathbf{x}^S(\mathbf{s}, t)^\top \boldsymbol{\beta}^S + \mathbf{x}^{NS}(\mathbf{s}, t)^\top \boldsymbol{\beta}_{mean}^{NS} + u^S(\mathbf{s}, t); \\ [y_{max}(\mathbf{s}, t) | \mu_{max}(\mathbf{s}, t), \sigma_{max}] &\sim \text{Gumbel}(\mu_{max}(\mathbf{s}, t), \sigma_{max}) \quad \text{with} \\ \mu_{max}(\mathbf{s}, t) &= \mathbf{x}^S(\mathbf{s}, t)^\top \boldsymbol{\beta}^S \beta_1^{Gaussian-Gumbel} \\ &\quad + \mathbf{x}^{NS}(\mathbf{s}, t)^\top \boldsymbol{\beta}_{max}^{NS} + \beta_2^{Gaussian-Gumbel} u^S(\mathbf{s}, t), \end{aligned} \quad (7)$$

where the terms $\boldsymbol{\beta}^S$ and $u^S(\mathbf{s}, t)$ with superscript S denote the sharing effects, and $\mathbf{x}^S(\mathbf{s}, t)$ are corresponding variables (geographical, meteorological and human-effect variables). The term $\boldsymbol{\beta}^{NS}$ with superscript NS denotes the non-sharing effects with corresponding covariates $\mathbf{x}^{NS}(\mathbf{s}, t)$ which includes the intercept and the location variables (longitude and latitude). For the specific selection of sharing and non-sharing variables, we treat all five main predictors (altitude, temperature, precipitation, vapour pressure and population density) as sharing terms in order to investigate the potential similar and different effects, and include the longitude and latitude as non-sharing terms to adjust the effects from different locations, which is consistent with the choice in the univariate generalised extreme value models, see Section 3.2. Additionally, the spatio-temporal random effect is also treated as sharing effects with respect to the simplicity of computation.

For further explanation, the sharing effects (including fixed effects and random effects) are approximately the same in two sub-models $(\boldsymbol{\beta}^S, u^S(\mathbf{s}, t))$. Meanwhile, they are linked by the sharing coefficients (scaling factors) $\beta_1^{Gaussian-Gumbel}$ and $\beta_2^{Gaussian-Gumbel}$. On the one hand, these sharing coefficients relax the strictly equal relation between the sharing effects in two sub-models. On the other hand, more importantly, their posterior distributions can also measure the similarities and differences in the effects of predictors in the sub-models. For instance, a significantly negative $\beta_1^{Gaussian-Gumbel}$ implies that the corresponding predictors oppositely influence the moderate and extreme air pollution cases.

3.4 Priors Definition

In a Bayesian context, in order to finalize the model we need to define prior distributions for the remaining parameters in Gumbel (σ_{Gumbel}) and GEV distributions (σ_{GEV}, ξ_{GEV}), the regression coefficients ($\boldsymbol{\beta}$), the sharing coefficients in

the joint model ($\beta^{Gaussian-Gumbel}$), parameters in the Matérn covariance function (σ_M, ρ_M, ν_M) and the parameters in AR(1) dynamic model (a, τ_{AR}).

We use vague Gaussian priors for the tail parameter (ξ_{GEV}) in GEV distribution and the elements of coefficients ($\beta, \beta^{Gaussian-Gumbel}$). The smooth parameter ν_M is treated here as a fixed value with $\nu_M = 1$, as in most spatial analyses. Note that INLA often uses the precision parameter (τ) to replace the scale parameter (σ) by $\sigma = 1/\sqrt{\tau}$, and we keep using gamma priors (INLA default priors) for the transformed precision parameters in Gumbel distribution (τ_{Gumbel}), GEV distribution (τ_{GEV}) and AR(1) model (τ_{AR}).

All other parameters, σ_M and ρ_M in the Matérn function and auto-correlation parameter a in AR(1) model are defined with the penalized complexity (PC) priors (Simpson et al., 2017). The penalised complexity (PC) prior is a weakly informative prior distribution, designed to punish model complexity by placing an exponential prior on the distance from some base models. PC priors for the range parameter (ρ_M) and standard deviation parameters (σ_M) can be defined with the guidance of Moraga (2019) in Matérn covariance function, ρ_M with $\text{Prob}(\rho_M < 10000) = 0.01$, which means the probability that the range is less than 10km is very small, and the prior for variance parameter as $\text{Prob}(\sigma_M > 3) = 0.01$, indicating the probability for variance greater than 3 is low. Similarly, we apply the auto-correlation (a) PC prior proposed in Simpson et al. (2017), following the recommendation of $\text{Prob}(a > 0) = 0.9$.

3.5 Model Evaluation, Diagnosis and Cross-validation

Traditional Bayesian model performance is evaluated by two popular criteria, the deviance information criterion (DIC) and the Watanabe-Akaike information criterion (WAIC). The deviance information criterion (DIC) proposed by Spiegelhalter et al. (2002), is a popular criterion for model choice similar to the Akaike information criterion (AIC).

$$DIC = D(\hat{\theta}) + 2p_D,$$

where $D(\hat{\theta})$ is the deviance function with Bayes estimate $\hat{\theta}$, and p_D is the effective number of parameters. The Watanabe-Akaike information criterion, also known as widely applicable Bayesian information criterion, is similar to the DIC but the effective number of parameters is computed in a different way (Watanabe, 2013).

However, DIC may under-penalize complex models with many random effects. Alternatively, for prediction performance, INLA suggests to apply the leave-one-out cross-validation criteria, conditional predictive ordinates (CPO; Pettit, 1990) and predictive integral transform (PIT; Marshall and Spiegelhalter, 2003), which facilitates the computation of the cross-validated log-score for model choice, and enables the calibration assessment of out-of-sample predictions, respectively.

$$\begin{aligned} CPO_i &= \pi(y_i^{\text{obs}} \mid y_{-i}), \\ PIT_i &= \text{Prob}(Y_i \leq y_i^{\text{obs}} \mid y_{-i}), \end{aligned}$$

where y_i^{obs} denotes the i -th observation and y_{-i} denotes the observations y with the i -th component omitted. However, numerical problems may occur when CPO and PIT values are computed with INLA algorithm (Held et al., 2010). With implementation in R-INLA package, some of the CPO and PIT values might not be reliable due to numerical problems, and R-INLA automatically stores a file which contains failure flags for each observation.

We also take a few other criteria introduced in Bayesian literature into account: The coverage probability of 95% CI is computed as the proportion of the validation observations that the observed value lies between the 2.5% quantile to the 97.5% quantile of the predicted value (posterior distribution). The correlation coefficient denotes the correlation between observed values and predicted values in the validation set. The root mean square error (RMSE) is defined as the square root of the second sample moment of the differences between predicted values and observed values.

As we separate the original five-year dataset (2017-2021) into training (2017-2020) and validation (2021) sets, we decide to apply DIC, WAIC, CPO, PIT and RMSE to compare the model fitness on the training set, and use the coverage probability, correlation coefficient, and RMSE for predictive ability evaluation.

4 Results

In this section, we firstly compare the performance of the Bayesian generalised extreme models and select the best with the outstanding predictive ability (Section 4.1), then summarize the corresponding posterior estimates for both fixed and random effects (Section 4.2). We also bring the best model into excursion functions generation with severe air pollution risk ranking (Section 4.3) and analyze the joint model outputs to give interpretation (Section 4.4). Note that since the explanatory variables are measured in different scales, to avoid numerical problems, each predictor is standardized to have mean zero and unit standard deviation.

4.1 Model comparison

In order to examine the fitting and prediction ability of the extreme value models, we apply some evaluation criteria (DIC, WAIC, CPO, PIT and RMSE) on training set (Table 3), and use other criteria (coverage probability, correlation and RMSE) on the validation set (Table 4). In Table 3, Model 1 and Model 3 outperform in DIC (229.78 and 277.48, respectively), WAIC (356.86 and 317.67, respectively) and RMSE (0.24 and 0.23, respectively), but Model 2 and Model 4 are more preferable in CPO (1546.14 and 734.45, respectively). In Table 4, Model 1 and Model 3 show much greater performance with the coverage probability (83.95%; 83.90%) and the RMSE (0.36; 0.37), but become less competitive with correlation (40.95%; 37.21%).

In terms of the PIT plots on the training set (Figure 3), which favours the shape of uniform distribution, Model 2 shows dominantly better performance than the others. Figure 4 shows the simultaneous visualization of model performance on both training and validation sets, where the horizontal axis represents the observed values and the vertical axis represents the estimated (predicted) values. The scatters distributed along the line with intercept 0 and slope 1 means the estimated (predicted) values are best suited to the observations. Model 1 and Model 3 generally perform better, because Model 2 and Model 4 usually produce relatively lower estimated (predicted) values against increasing observed values.

To summary, although no model excels in all categories of criteria, Model 1 (the Gumbel model with fixed effects and spatio-temporal random effects defined in Eq.(2)) generally gives a satisfactory result in most circumstances (DIC, WAIC, RMSE, coverage probability, correlation and the visualization plot). As a result, we choose Model 1 as the best model and takes it into further analysis.

Table 3: Performance evaluation criteria (DIC, WAIC, CPO and RMSE) of Models 1~ 4 specified in Eqs.(2), (4)-(6) on the training set (all criteria prefer lower values).

Model	DIC	WAIC	CPO	RMSE
Model 1	229.78	356.86	8019.07	0.24
Model 2	777.16	854.86	1546.14	0.36
Model 3	277.48	317.67	12128.54	0.23
Model 4	781.98	799.40	734.45	0.33

Table 4: Performance evaluation criteria (coverage probability, correlation and RMSE) of Models 1~ 4 specified in Eqs.(2), (4)-(6) on the validation set. High coverage probability, high correlation, and low RMSE indicate the preferable model.

Model	Coverage Probability	Correlation	RMSE
Model 1	83.95%	40.95%	0.36
Model 2	58.88%	48.20%	0.48
Model 3	83.90%	37.21%	0.37
Model 4	60.78%	48.28%	0.48

4.2 Summary of Model 1

The summary statistics for fixed effects are shown in Table 5. For explanatory variables, altitude and population density are significantly negatively associated with annual maxima PM_{10} concentrations, whereas the coefficients for other covariates are not statistically significant. High temperature, low precipitation and low vapour pressure are likely to associate with extreme PM_{10} concentrations.

The spatial and temporal dependence is accessible by spatial heat plot (Figure 5) and posterior estimates of auto-correlation coefficient (a in Table 6). Spatially, similar values of mean random effects occur in groups, especially, a large cluster of high values happens in the centre of the mainland. Temporally, the estimated mean correlation coefficient (a) is 0.80 with 95% credible interval (0.74, 0.85), providing evidence of relatively strong dependence between two consecutive years.

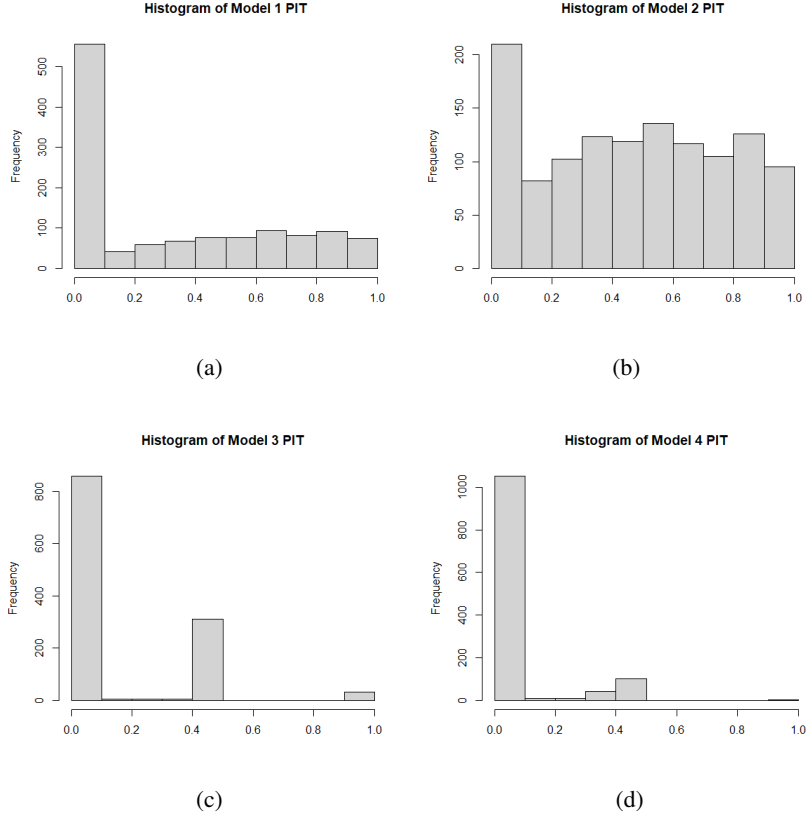


Figure 3: Predictive integral transform plots for Models 1 ~ 4 specified in Eqs.(2), (4)-(6) in (a)~(b) based on training dataset. A uniform distribution pattern is preferable.

Table 5: Posterior estimates (mean, standard deviation and quantiles) of the coefficients of the covariates involved in Model 1 specified in Eq.(2).

Covariate	Mean	Stdev	0.025 quantile	0.5 quantile	0.975 quantile
Intercept	4.20	0.12	3.96	4.20	4.43
Longitude	-0.08	0.13	-0.33	-0.08	0.17
Latitude	-0.06	0.13	-0.31	-0.06	0.19
Altitude	-0.08	0.03	-0.13	-0.08	-0.03
Temperature	0.13	0.10	-0.07	0.13	0.32
Precipitation	-0.03	0.06	-0.15	-0.03	0.09
Vapour Pressure	-0.09	0.09	-0.27	-0.09	0.09
Population Density	-0.07	0.03	-0.13	-0.07	-0.01

Table 6: Posterior estimates of mean, standard deviation and quantiles of the parameters in Model 1 specified in Eq.(2). The precision (τ_G) for Gumbel distribution, the range parameter (ρ_M) and the standard deviation (σ_M) introduced in Matérn covariance function and the auto-correlation coefficient (a).

Parameter	Mean	Stdev	0.025 quantile	0.5 quantile	0.975 quantile
Precision (τ_G)	25.62	1.64	22.52	25.57	28.99
Range (ρ_M , unit 10^5)	2.62	0.37	1.96	2.60	3.43
Stdev (σ_M)	0.58	0.05	0.48	0.57	0.69
Auto-correlation (a)	0.80	0.03	0.74	0.80	0.85

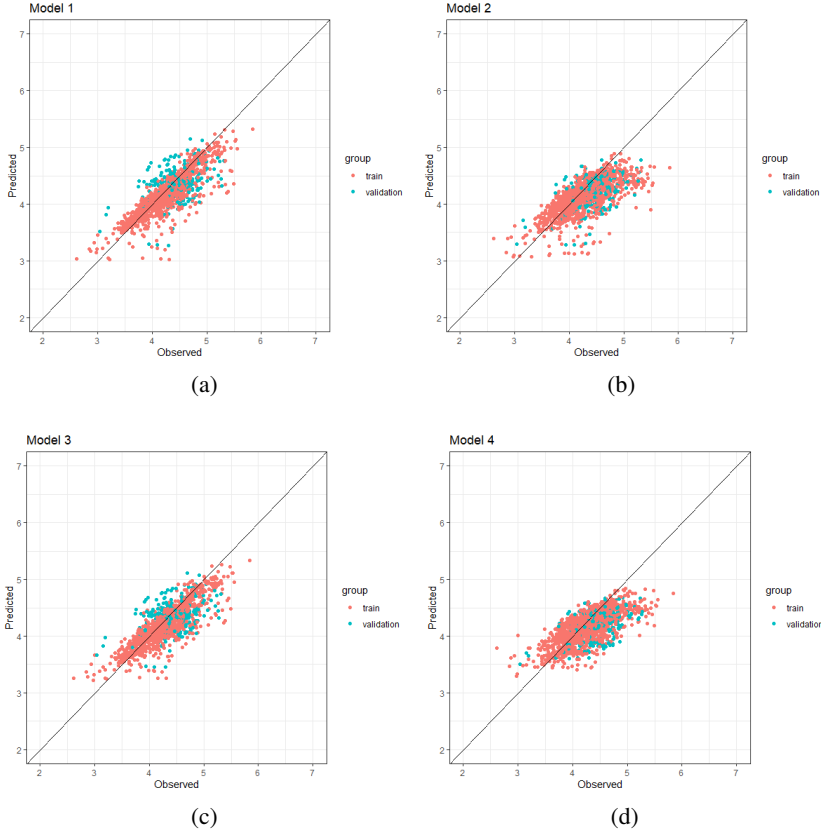


Figure 4: Visualisation of training (red) and validation (cyan) performance in (a)~(b) for Models 1~4 specified in Eqs.(2), (4)–(6) subsequently. The scatters distributed along the line with the intercept 0 and the slope denotes the better model.

4.3 Annual maxima prediction and excursion functions

Hot-spot region identifications and predictive concentration level plots are important tools in air pollution studies, because they intuitively imply the air quality in specific regions and are easily interpreted to environmental agencies and the general public. [Bolin and Lindgren \(2015\)](#) proposed the positive ($E_{u,\alpha}^+(X)$) and negative excursion sets ($E_{u,\alpha}^-(X)$) that determine the largest set that simultaneously exceeds or below the risk level (u) with a small error probability (α), employing a parametric family and sequential importance sampling method for estimating joint probabilities. To visualize the excursion sets simultaneously, we apply the positive and negative excursion functions, $F_u^+(s) = 1 - \inf \{\alpha \mid s \in E_{u,\alpha}^+\}$ and $F_u^-(s) = 1 - \inf \{\alpha \mid s \in E_{u,\alpha}^-\}$. To explain, the term $\inf \{\alpha \mid s_0 \in E_{u,\alpha}^+\}$ denotes the "smallest" α required that the location (s_0) can be included into the positive excursion set $E_{u,\alpha}^+$ at the first time, while the higher $1 - \inf \{\alpha \mid s_0 \in E_{u,\alpha}^+\}$ reported by positive excursion function generally indicates higher probabilities for the location (s_0) to exceed the risk threshold u simultaneously.

In our case, to discover areas that are most likely and most unlikely to suffer from severe PM₁₀ pollution simultaneously, we utilize predicted PM₁₀ concentration levels from Model 1 to generate both positive and negative excursion functions with the thresholds 50 $\mu\text{g}/\text{m}^3$ (poor) and 100 $\mu\text{g}/\text{m}^3$ (very poor) at 548 locations distributed throughout the mainland of Spain, including a set of $0.5^\circ \times 0.5^\circ$ (50km \times 50km) grids (206 locations) and locations of all PM₁₀ stations (342 monitors).

In the case of exceeding 50 $\mu\text{g}/\text{m}^3$ (Figure 6), the probability for simultaneously exceeding is high in the northwest, middle, and south, meaning that poor PM₁₀ pollution probably hazard these locations during the year. In contrast, the negative excursion function with threshold 50 $\mu\text{g}/\text{m}^3$ indicates that the regions in the north and east enjoy good or moderate air quality throughout the whole year. In the case of 100 $\mu\text{g}/\text{m}^3$ (Figure 7), the probabilities for very poor PM₁₀ pollution occurrence are low (in white) in most regions, but still likely to appear in certain areas in the

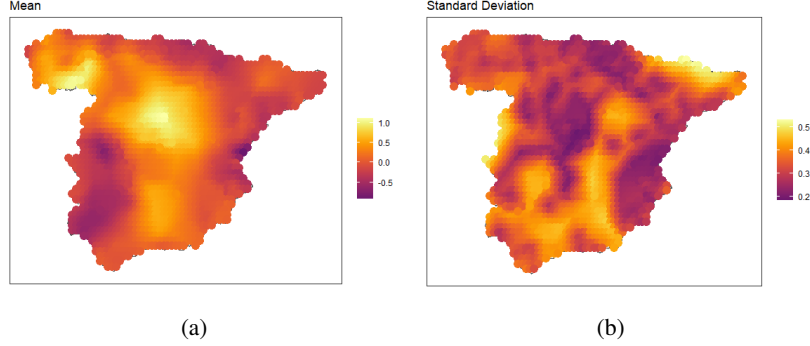


Figure 5: Heat map of spatial random effect with (a) mean and (b) standard deviation.

community of Madrid as well as the border between Galicia and Castile and León, meanwhile, most areas in the north, northeast and east are expected to be below this threshold.

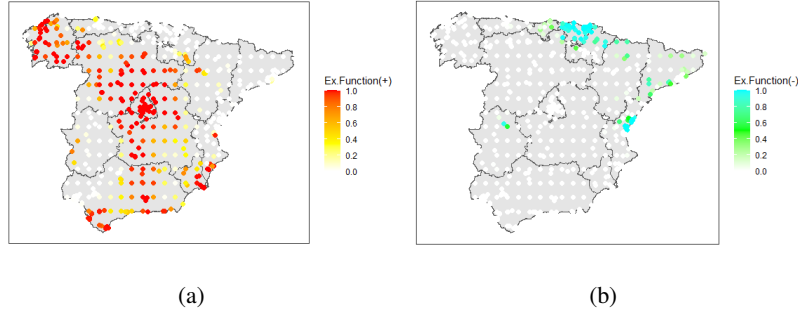


Figure 6: Positive and negative excursion functions with threshold $50 \mu\text{g}/\text{m}^3$ are displayed in (a) and (b), respectively. Annual maximum concentration level for locations in red are likely to exceed $50 \mu\text{g}/\text{m}^3$, and concentration level for locations in cyan are probably below the threshold.

4.4 Results of the joint model with sharing effects

Combining the best extreme value model (Model 1) with the Gaussian model, we establish the joint model in Section 3.3 with sharing effects to estimate both maxima and mean concentration levels simultaneously. Posterior estimates of sharing fixed effects with corresponding explanatory variables (altitude, temperature, precipitation, vapour pressure and population density) are shown in Table 7. Precipitation shows significant negative associations with both annual mean and annual maxima concentrations, indicating the PM_{10} concentrations are generally low in wet regions. In contrast, both altitude and temperature seem negatively connected with mean concentrations but positively connected with maxima concentrations, although the effects of temperature are not significant with respect to 95% credible interval. This result implies that locations with high altitudes and high temperatures enjoy generally better air quality but are more likely to suffer from extreme pollution in certain days.

Similarly, the plots of the posterior distributions of the sharing coefficients ($\beta_1^{\text{Gaussian-Gumbel}}$; introduced in Section 3.3) in Figure 8 suggests similar results of associations in Table 7. The posterior distribution of the precipitation coefficient almost lies between 0 and 1, showing that the influence of precipitation on extreme pollution is similar to the case of moderate pollution. Both the coefficients for altitude and temperature seem to be negative, showing evidence that altitude and temperature can impact inversely in two types of pollution. The other coefficients (population density and vapour pressure) are likely to be positive, but the credibility is relatively low.

As for model performance evaluation, the joint model performed well in the fitness of the training set, achieving -517.62 in DIC, -515.41 in WAIC and -201.49 in CPO. These values are far smaller than those for the univariate

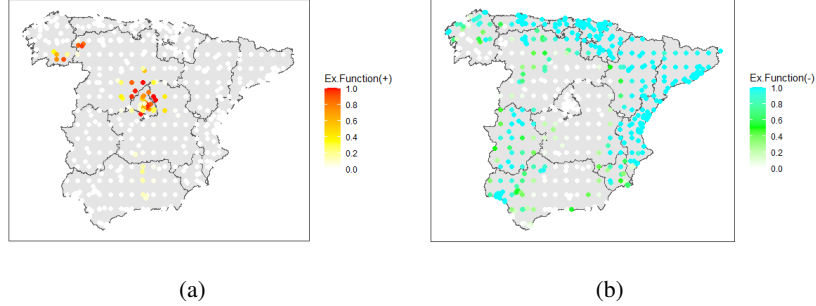


Figure 7: Positive and negative excursion functions with threshold $100 \mu\text{g}/\text{m}^3$ are displayed in (a) and (b), respectively. Annual maximum concentration levels for locations in red are likely to exceed $100 \mu\text{g}/\text{m}^3$, and concentration levels for locations in cyan are probably below the threshold.

Gumbel model specified in Eq.(2). This is because the assessment criteria take into account both sub-models (Gaussian and Gumbel) at the same time and the better fitted Gaussian model for the annual mean PM_{10} may help the extreme Gumbel model through the sharing effects. To be specific, Table 8 and Figure 9 provide insight into the validation performance of the two sub-models, where the performance of the Gumbel model (maxima model) is relatively good but less comparable to the Gaussian model (mean model). Although the less parsimony joint model might give rise to more volatility in prediction for the extreme sub-model, the satisfying evaluation results still enhance the credibility of the results and findings of the joint model. In particular, the prediction ability is improved with increased correlation as 56.10% and the PIT plot tends to be uniform distributed in the joint model, see details in Table 8 and Figure 9(a).

Table 7: Posterior estimates (mean and 95% credible interval) of the sharing effects and non-sharing effects specified in Eq.(7).

Covariate	Annual mean model (β^S)		Annual maxima model ($\beta^S \beta_1^{\text{Gaussian-Gumbel}}$)	
	Mean	95% Credible Interval	Mean	95% Credible Interval
Altitude	-0.126	(-0.153, -0.099)	0.026	(0.020, 0.032)
Temperature	-0.046	(-0.104, 0.011)	0.007	(-0.002, 0.016)
Precipitation	-0.098	(-0.122, -0.075)	-0.046	(-0.073, -0.044)
Vapour Pressure	-0.005	(-0.060, 0.050)	-4.559×10^{-5}	(-0.003, 0.003)
Population Density	-0.019	(-0.050, 0.011)	-0.004	(-0.011, 0.003)
Covariate	Annual mean model ($\beta_{\text{mean}}^{\text{NS}}$)		Annual maxima model ($\beta_{\text{max}}^{\text{NS}}$)	
	Mean	95% Credible Interval	Mean	95% Credible Interval
Intercept	2.781	(2.733, 2.829)	4.019	(3.976, 4.062)
Longitude	-0.007	(-0.056, 0.042)	-0.059	(-0.103, -0.015)
Latitude	-0.082	(-0.137, -0.027)	-0.073	(-0.118, -0.028)

Table 8: Sub-models performance evaluation (coverage probability, correlation and RMSE) in the validation set.

Sub-model	Coverage Probability	Correlation	RMSE
Gaussian Model (Mean)	78.82%	84.01%	0.191
Gumbel Model (Maxima)	20.78%	56.10%	1.618

5 Discussions and Conclusions

In this paper, we apply the PM_{10} concentrations data in mainland Spain to our models for three main reasons. Firstly, Spain is a mountainous country with a large central plateau, and this complicated orography is usually associated with

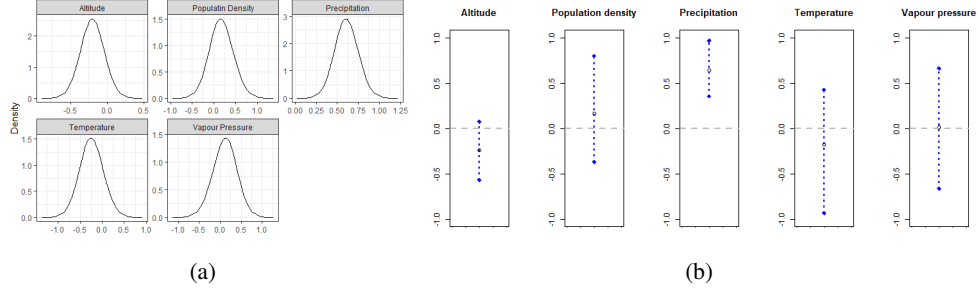


Figure 8: (a) The posterior distributions plot and (b) the quantiles plot of sharing coefficients. The three nodes in the quantiles plot indicate 0.025, 0.5, and 0.975 quantiles of the posterior estimates.

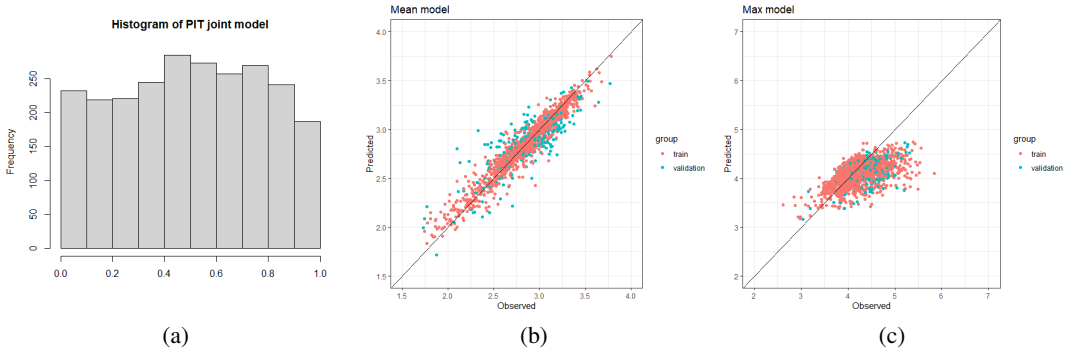


Figure 9: (a) Histogram of PIT for joint model defined in Eq.(7) on training set, (b) the mean sub-model and (c) the max sub-model performance in both training and validation sets.

a variety of climatic conditions. Secondly, the air pollution monitors distributed throughout mainland Spain provide high-quality time series data, which supports both local and national level accurate prediction and credible inference. Finally, Spain generally enjoys good air quality (low annual mean), but extreme air pollution does appear on certain days during the year (high annual maxima). This circumstance allows us to investigate the potential difference in the generation and spread of the moderate and extreme cases.

We establish a series of Bayesian spatio-temporal models on extreme PM_{10} concentrations in Spain, with specifically meteorological predictors, human effects, and spatio-temporal random effects following SPDE and AR(1) dynamic to account for the dependence not explained by covariates. We also generate the annual maxima excursion functions maps specified at the grid level to highlight the regional risk ranking, as well as provide certain evidence in similar and different connections between influential predictors and different scaled PM_{10} concentrations by Bayesian joint model with sharing effects.

Although most statistical studies focus on moderate cases with long-term exposure, in epidemiological field, short-term exposures to severe particulate matter is considered to be an important public health issue with major acute cardiovascular problems and health economic consequences. For example, [Brook et al. \(2016\)](#) emphasized that people living in highly polluted regions probably increase heart failure hospitalisations and cardiovascular mortality several folds. [Shah et al. \(2013\)](#) also pointed out that even modest improvements in air quality are projected to have major population health benefits and substantial health-care cost savings, preventing thousands of heart failure hospitalisations and saving millions of US dollars a year.

Combined with these health and economic hazards, the main findings in this paper are expected to provide in-depth knowledge of extreme air pollution spreading, promote awareness of extreme studies, and provide suggestions to the national governments in the legislation of extremely poor air quality regulation and human health protection. In particular, the Bayesian joint model with sharing effects highlights the inverse effects of altitude and temperature on moderate and extreme PM_{10} pollution cases, which is expected to reveal the difference in the generation and spread of different scaled PM_{10} pollution. Moreover, the excursion functions maps imply the central and northwest regions in Spain are more likely to suffer from severe PM_{10} pollution, which can be applied in research of long-term effects

and health outcomes in epidemiological studies, such as acute cardiovascular events (Mustafić et al., 2012; Shah et al., 2013) and various types of strokes (Yu et al., 2014).

As for main limitations, firstly, previous air pollution studies indicate that the generation and spread of particulate matter are associated with various meteorological variables and human-made effects, such as temperature, wind speed, as well as transport and burning emissions. However, time-series data with high-resolution records are generally limited and inaccessible for both kinds of factors, which is the main reason for the limited number of explanatory variables in our study. Improved predictors collection can consider human-made factors such as "daily emissions" (Cameletti et al., 2013) and "linear distance to the nearest highway" (Fioravanti et al., 2021), as well as the meteorological variable records with aggregation on the specific periods when the maxima air pollution observations occurred. Secondly, our study only focuses on a five-year period to reduce the computation burden for conducting the Bayesian spatio-temporal model on a national scale, but the short-period scenario makes detecting the long-term temporal pattern to be challenging. Finally, in analysis with point data, dispersion is evaluated as the dependent of the boundary, because spatial data can appear either dispersed or clustered depending on the boundary. In this study, since the common approaches to adjusting edge effects usually result in large-area statistics that increase the computational complexity, we decide to keep the assumption of an infinite surface in which the edge effects do not occur (ignorance of boundary problem).

References

Agarwal, A. and Kaddoura, I. (2019). On-road air pollution exposure to cyclists in an agent-based simulation framework. *Periodica Polytechnica Transportation Engineering*, 48(2):117–125.

Amin, N. A. M., Adam, M. B., and Aris, A. Z. (2015). Bayesian extreme for modeling high PM₁₀ concentration in Johor. *Procedia Environmental Sciences*, 30:309–314.

Balkema, A. and Haan, L. (1974). Residual life time at great age. *The Annals of Probability*, 2.

Basnayake, K., Mazaad, D., Bemelmans, A., Rouach, N., Korkotian, E., and Holcman, D. (2019). Fast calcium transients in dendritic spines driven by extreme statistics. *PLOS Biology*, 17:e2006202.

Beirlant, J., Goegebeur, Y., Teugels, J., and Segers, J. (2005). *Statistics of Extremes: Theory and Applications*. Wiley.

Beloconi, A., Chrysoulakis, N., Lyapustin, A. I., Utzinger, J., and Vounatsou, P. (2018). Bayesian geostatistical modelling of PM₁₀ and PM_{2.5} surface level concentrations in Europe using high-resolution satellite-derived products. *Environment International*, 121:57–70.

Blangiardo, M., Cameletti, M., Baio, G., and Rue, H. (2013). Spatial and spatio-temporal models with R-INLA. *Spatial and Spatio-temporal Epidemiology*, 7:39–55.

Blondel, V. D., Guillaume, J. L., Lambiotte, R., and Lefebvre, E. (2008). Fast unfolding of communities in large networks. *J. Stat. Mech.-Theory Exp.*, 2008:P10008.

Bolin, D. and Lindgren, F. (2015). Excursion and contour uncertainty regions for latent Gaussian models. *Journal of the Royal Statistical Society Series B (Statistical Methodology)*, 77:85–106.

Bolin, D. and Wallin, J. (2019). Scale dependence: Why the average CRPS often is inappropriate for ranking probabilistic forecasts. *arXiv: Statistics Theory*.

Brook, R. D., Sun, Z., Brook, J. R., Zhao, X., Ruan, Y., Yan, J., Mukherjee, B., Rao, X., Duan, F., Sun, L., Liang, R., Lian, H., Zhang, S., Fang, Q., Gu, D., Sun, Q., Fan, Z., and Rajagopalan, S. (2016). Extreme air pollution conditions adversely affect blood pressure and insulin resistance: The air pollution and cardiometabolic disease study. *Hypertension*, 67(1):77–85.

Bucher, A. and Segers, J. (2017). Inference for heavy tailed stationary time series based on sliding blocks. *Electronic Journal of Statistics*, 12:1098–1125.

Cameletti, M., Lindgren, F., Simpson, D., and Rue, H. (2013). Spatio-temporal modeling of particulate matter concentration through the SPDE approach. *AStA Advances in statistical analysis: A journal of the German Statistical Society*, 97(2):109–131.

Cao, W. and Zhang, Z. (2020). New extreme value theory for maxima of maxima. *Statistical Theory and Related Fields*, 5:1–21.

Castro-Camilo, D., Huser, R., and Rue, H. (2021). Practical strategies for generalized extreme value-based regression models for extremes. *Environmetrics*, 33(6):e2742.

Chen, Q., Wu, T. T., and Fang, M. (2013). Detecting local community structure in complex networks based on local degree central nodes. *Physica A*, 392:529–537.

Chu, H., Huang, B., and Lin, C. (2015). Modeling the spatio-temporal heterogeneity in the PM₁₀-PM_{2.5} relationship. *Atmospheric Environment*, 102:176–182.

Clauset, A., Newman, M. E. J., and Moore, C. (2004). Finding community structure in very large networks. *Phys. Rev. E*, 70:066111.

Cohen, A. J., Brauer, M., Burnett, R., Anderson, H. R., Frostad, J., Estep, K., Balakrishnan, K., Brunekreef, B., Dandona, L., Dandona, R., Feigin, V., Freedman, G., Hubbell, B., Jobling, A., Kan, H., Knibbs, L., Liu, Y., Martin, R., Morawska, L., Pope, C. A., Shin, H., Straif, K., Shaddick, G., Thomas, M., van Dingenen, R., van Donkelaar, A., Vos, T., Murray, C. J. L., and Forouzanfar, M. H. (2017). Estimates and 25-year trends of the global burden of disease attributable to ambient air pollution: An analysis of data from the global burden of diseases study 2015. *The Lancet*, 389(10082):1907–1918.

Coles, S. (2001). *An Introduction to Statistical Modeling of Extreme Values*, volume 97. Springer.

Copat, C., Cristaldi, A., Fiore, M., Grasso, A., Zuccarello, P., Signorelli, S. S., Conti, G. O., and Ferrante, M. (2020). The role of air pollution (PM and NO₂) in COVID-19 spread and lethality: A systematic review. *Environmental Research*, 191:110129.

Costa, V. and Sampaio, J. (2021). Bayesian approach for estimating the distribution of annual maximum floods with a mixture model. *Journal of Hydrologic Engineering*, 26:04021017.

Cumperayot, P. and Kouwenberg, R. (2013). Early warning systems for currency crises: A multivariate extreme value approach. *Journal of International Money and Finance*, 36:151–171.

Daellenbach, K., Uzu, G., Jiang, J., Cassagnes, L.-E., Leni, Z., Vlachou, A., Stefanelli, G., Canonaco, F., Weber, S., Segers, A., Kuenen, J., Schaap, M., Favez, O., Albinet, A., Aksoyoglu, S., Dommen, J., Baltensperger, U., Geiser, M., Haddad, I., and Prevot, A. (2020). Sources of particulate-matter air pollution and its oxidative potential in Europe. *Nature*, 587:414–419.

Danon, L., Diaz-Guilera, A., Duch, J., and Arenas, A. (2005). Comparing community structure identification. *J. Stat. Mech.-Theory Exp.*, page P09008.

Davison, A. C. and Smith, R. L. (1990). Models for exceedances over high thresholds. *Journal of the Royal Statistical Society Series B-Methodological*, 52:393–425.

Dias, D. and Tchepel, O. (2018). Spatial and temporal dynamics in air pollution exposure assessment. *International Journal of Environmental Research and Public Health*, 15(3):558.

Ding, Y., Cheng, B., and Jiang, Z. (2008). A newly-discovered GPD-GEV relationship together with comparing their models of extreme precipitation in summer. *Advances in Atmospheric Sciences*, 25:507–516.

Fabio, D. R., Fabio, D., and Carlo, P. (2013). Profiling core-periphery network structure by random walkers. *Sci. Rep.*, 3:1467.

Fabricio, B. and Liang, Z. (2013). Fuzzy community structure detection by particle competition and cooperation. *Soft Comput.*, 17:659–673.

Fioravanti, G., Martino, S., Cameletti, M., and Cattani, G. (2021). Spatio-temporal modelling of PM₁₀ daily concentrations in Italy using the SPDE approach. *Atmospheric Environment*, 248:118192.

Fisher, R. and Tippett, L. (1928a). Limiting forms of the frequency distribution of the largest or smallest member of a sample. *Mathematical Proceedings of the Cambridge Philosophical Society*, 24:180–190.

Fisher, R. A. and Tippett, L. H. C. (1928b). Limiting forms of the frequency distribution of the largest or smallest member of a sample. *Mathematical Proceedings of the Cambridge Philosophical Society*, 24(2):180–190.

Forlani, C., Bhatt, S., Cameletti, M., Krainski, E., and Blangiardo, M. (2020). A joint Bayesian space-time model to integrate spatially misaligned air pollution data in R-INLA. *Environmetrics*, 31(8):e2644.

Fortunato, S. (2010). Community detection in graphs. *Phys. Rep.-Rev. Sec. Phys. Lett.*, 486:75–174.

Fortunato, S. and Barthelemy, M. (2007). Resolution limit in community detection. *Proc. Natl. Acad. Sci. U. S. A.*, 104:36–41.

Fuglstad, G.-A., Simpson, D., Lindgren, F., and Rue, H. (2019). Constructing priors that penalize the complexity of Gaussian random fields. *Journal of the American Statistical Association*, 114(525):445–452.

Gandhi, V. (2015). *Brain-Computer Interfacing for Assistive Robotics*, pages 7–63. Academic Press, San Diego.

Gelman, A., Meng, X.-L., and Stern, H. (1996). Posterior predictive assessment of model fitness via realized discrepancies. *Statistica Sinica*, 6(4):733–760.

Gembbris, D., Taylor, J. G., and Suter, D. (2007). Evolution of athletic records: Statistical effects versus real improvements. *Journal of Applied Statistics*, 34(5):529–545.

Genton, M. G. (2002). Classes of kernels for machine learning: A statistics perspective. *Journal of Machine Learning Research*, 2:299–312.

Gneiting, T. and Ranjan, R. (2011). Comparing density forecasts using threshold- and quantile-weighted scoring rules. *Journal of Business & Economic Statistics*, 29:411–422.

Gregory, S. (2011). Fuzzy overlapping communities in networks. *J. Stat. Mech.-Theory Exp.*, page P02017.

Guttorp, P. and Gneiting, T. (2006). Studies in the history of probability and statistics XLIX On the Matérn correlation family. *Biometrika*, 93(4):989–995.

Harris, I., Osborn, T. J., Jones, P., and Lister, D. (2020). Version 4 of the CRU TS monthly high-resolution gridded multivariate climate dataset. *Scientific data*, 7(1):109.

Havens, T. C., Bezdek, J. C., Leckie, C., R. K., and Palaniswami, M. (2013). A soft modularity function for detecting fuzzy communities in social networks. *IEEE Trans. Fuzzy Syst.*, 21:1170–1175.

Heffernan, J. and Tawn, J. (2004). A conditional approach for multivariate extreme values. *Journal of the Royal Statistical Society Series B*, 66:497–546.

Held, L., Schrödle, B., and Rue, H. (2010). *Posterior and Cross-validatory Predictive Checks: A Comparison of MCMC and INLA*, pages 91–110. Physica-Verlag HD, Heidelberg.

Huang, G., Blangiardo, M., Brown, P. E., and Pirani, M. (2021). Long-term exposure to air pollution and COVID-19 incidence: A multi-country study. *Spatial and Spatio-temporal Epidemiology*, 39:100443.

Huang, G., Lee, D., and Scott, E. M. (2018). Multivariate space-time modelling of multiple air pollutants and their health effects accounting for exposure uncertainty. *Statistics in Medicine*, 37:1134 – 1148.

Hullermeier, E. and Rifqi, M. (2009). A fuzzy variant of the rand index for comparing clustering structures. In *in Proc. IFSA/EUSFLAT Conf.*, pages 1294–1298.

Joseph, A., Sawant, A., and Srivastava, A. (2003). PM₁₀ and its impacts on health - a case study in Mumbai. *International Journal of Environmental Health Research*, 13(2):207–214.

Joseph, M. B., Rossi, M. W., Mietkiewicz, N. P., Mahood, A. L., Cattau, M. E., St. Denis, L. A., Nagy, R. C., Iglesias, V., Abatzoglou, J. T., and Balch, J. K. (2019). Spatiotemporal prediction of wildfire size extremes with Bayesian finite sample maxima. *Ecological Applications*, 29(6):e01898.

Katzfuss, M. (2013). Bayesian nonstationary spatial modeling for very large datasets. *Environmetrics*, 24(3):189–200.

Kjeldsen, T. R., Ahn, H., Prosdocimi, I., and Heo, J.-H. (2018). Mixture Gumbel models for extreme series including infrequent phenomena. *Hydrological Sciences Journal*, 63(13-14):1927–1940.

Koh, J., Pumont, F., Dupuy, J., and Opitz, T. (2021). Spatiotemporal wildfire modeling through point processes with moderate and extreme marks. *The Annals of Applied Statistics*, in press, <https://doi.org/10.48550/arXiv.2105.08004>.

Lancichinetti, A. and Fortunato, S. (2009). Benchmarks for testing community detection algorithms on directed and weighted graphs with overlapping communities. *Phys. Rev. E.*, 80:016118.

Lancichinetti, A., Fortunato, S., and Radicchi, F. (2008). Benchmark graphs for testing community detection algorithms. *Phys. Rev. E.*, 78:046110.

Lenschow, P., Abraham, H.-J., Kutzner, K., Lutz, M., Preuß, J.-D., and Reichenbächer, W. (2001). Some ideas about the sources of PM₁₀. *Atmospheric Environment*, 35:S23–S33.

Li, J., Wang, X., and Eustace, J. (2013). Detecting overlapping communities by seed community in weighted complex networks. *Physica A.*, 392:6125–6134.

Lindgren, F. and Rue, H. (2015). Bayesian spatial modelling with R-INLA. *Journal of Statistical Software*, 63:1–25.

Lindgren, F., Rue, H., and Lindström, J. (2011). An explicit link between Gaussian fields and Gaussian Markov random fields: The Stochastic Partial Differential Equation approach. *Journal of the Royal Statistical Society: Series B (Statistical Methodology)*, 73(4):423–498.

Liu, J. (2010). Fuzzy modularity and fuzzy community structure in networks. *Eur. Phys. J. B.*, 77:547–557.

Liu, W., Pellegrini, M., and Wang, X. (2014). Detecting communities based on network topology. *Sci. Rep.*, 4:5739.

Lou, H., Li, S., and Zhao, Y. (2013). Detecting community structure using label propagation with weighted coherent neighborhood propinquity. *Physica A.*, 392:3095–3105.

Maposa, D., Seimela, A., Sigauke, C., and Cochran, J. (2021). Modelling temperature extremes in the Limpopo province: Bivariate time-varying threshold excess approach. *Natural Hazards*, 107.

Marshall, E. C. and Spiegelhalter, D. J. (2003). Approximate cross-validatory predictive checks in disease mapping models. *Statistics in Medicine*, 22(10):1649–1660.

Martins, L. D., Wikuats, C. F. H., Capucim, M. N., de Almeida, D. S., da Costa, S. C., Albuquerque, T., Barreto Carvalho, V. S., de Freitas, E. D., de Fátima Andrade, M., and Martins, J. A. (2017). Extreme value analysis of air pollution data and their comparison between two large urban regions of South America. *Weather and Climate Extremes*, 18:44–54.

Martuzzi, M., Mitis, F., Iavarone, I., and Serinelli, M. (2006). *Health impact of PM₁₀ and ozone in 13 Italian cities*. World Health Organization. Regional Office for Europe.

Matérn, B. (1986). *Spatial variation*, volume 36. Springer New York.

Moraga, P. (2019). *Geospatial Health Data: Modeling and Visualization with R-INLA and Shiny*. Chapman & Hall/CRC Biostatistics Series.

Moraga, P., Dean, C., Inoue, J., Morawiecki, P., Noureen, S., and Wang, F. (2021). Bayesian spatial modelling of geostatistical data using inla and spde methods: A case study predicting malaria risk in mozambique. *Spatial and Spatio-temporal Epidemiology*, 39:100440.

Mustafić, H., Jabre, P., Caussin, C., Murad, M. H., Escolano, S., Tafflet, M., Périer, M.-C., Marijon, E., Vernerey, D., Empana, J.-P., and Jouven, X. (2012). Main air pollutants and myocardial infarction: A systematic review and meta-analysis. *Journal of the American Medical Association*, 307(7):713–721.

Nepusz, T., Petróczi, A., Négyessy, L., and Bazsó, F. (2008). Fuzzy communities and the concept of bridgeness in complex networks. *Phys. Rev. E.*, 77:016107.

Newman, M. E. J. (2013). Network data. <http://www-personal.umich.edu/~mejn/netdata/>.

Newman, M. E. J. and Girvan, M. (2004). Finding and evaluating community structure in networks. *Phys. Rev. E.*, 69:026113.

Omidvarborna, H., Kumar, A., and Kim, D.-S. (2015). Recent studies on soot modeling for diesel combustion. *Renewable and Sustainable Energy Reviews*, 48:635–647.

Opitz, T., Huser, R., Bakka, H., and Rue, H. (2018). INLA goes extreme: Bayesian tail regression for the estimation of high spatio-temporal quantiles. *Extremes*, 21(3):441–462.

Pettit, L. (1990). The conditional predictive ordinate for the Normal distribution. *Journal of the Royal Statistical Society: Series B (Methodological)*, 52(1):175–184.

Pickands, J. (1971). The two-dimensional Poisson process and extremal processes. *Journal of Applied Probability*, 8(4):745–756.

Pickands, J. (1975). Statistical inference using extreme order statistics. *The Annals of Statistics*, 3(1):119 – 131.

Porcu, E., Montero, J., and Schlather, M. (2012). *Advances and Challenges in Space-time Modelling of Natural Events*. Springer.

Psorakis, I., Roberts, S., Ebden, M., and Sheldon, B. (2011). Overlapping community detection using bayesian non-negative matrix factorization. *Phys. Rev. E*, 83:066114.

Raghavan, U., Albert, R., and Kumara, S. (2007). Near linear time algorithm to detect community structures in large-scale networks. *Phys. Rev E*, 76:036106.

Reiss, R.-D. and Thomas, M. (2007). Statistical analysis of extreme values with applications to insurance, finance, hydrology and other fields. *Journal of the American Statistical Association*, 93.

Resnick, S. and Starica, C. (1997). Smoothing the Hill estimator. *Advances in Applied Probability*, 29:271–293.

Rue, H., Martino, S., and Chopin, N. (2009). Approximate Bayesian inference for latent Gaussian models by using Integrated Nested Laplace Approximations. *Journal of the Royal Statistical Society: Series B (Statistical Methodology)*, 71(2):319–392.

Rue, H., Riebler, A., Sørbye, S., Illian, J., Simpson, D., and Lindgren, F. (2016). Bayesian computing with INLA: A review. *Annual Review of Statistics and Its Application*, 4.

Sahu, S. K. (2012). Hierarchical Bayesian models for space-time air pollution data. *Handbook of Statistics*, 30:477–495.

Samoli, E., Stafloggia, M., Rodopoulou, S., Ostro, B., Declercq, C., Alessandrini, E., Díaz, J., Karanasiou, A., Kelessis, A. G., Tertre, A. L., Pandolfi, P., Randi, G., Scarinzi, C., Zauli-Sajani, S., Katsouyanni, K., and Forastiere, F. (2013). Associations between fine and coarse particles and mortality in Mediterranean cities: Results from the MED-PARTICLES Project. *Environmental Health Perspectives*, 121(8):932–938.

Sario, M. D., Katsouyanni, K., and Michelozzi, P. (2013). Climate change, extreme weather events, air pollution and respiratory health in Europe. *The European respiratory journal*, 42(3):826—843.

Setti, L., Passarini, F., De Gennaro, G., Barbieri, P., Pallavicini, A., Ruscio, M., Piscitelli, P., Colao, A., and Miani, A. (2020). Searching for SARS-COV-2 on particulate matter: A possible early indicator of COVID-19 epidemic recurrence. *International Journal of Environmental Research and Public Health*, 17(9).

Sevinc, V., Kucuk, O., and Goltas, M. (2020). A Bayesian network model for prediction and analysis of possible forest fire causes. *Forest Ecology and Management*, 457:117723.

Shah, A. S., Langrish, J. P., Nair, H., McAllister, D. A., Hunter, A. L., Donaldson, K., Newby, D. E., and Mills, N. L. (2013). Global association of air pollution and heart failure: A systematic review and meta-analysis. *The Lancet*, 382(9897):1039–1048.

Sharma, P., Chandra, A., Kaushik, S., Sharma, P., and Jain, S. (2012). Predicting violations of national ambient air quality standards using extreme value theory for Delhi city. *Atmospheric Pollution Research*, 3(2):170–179.

Shumway, R. H. and Stoffer, D. S. (2011). *Time Series Analysis and Its Applications: With R Examples*, volume 9. Springer Cham.

Simpson, D., Rue, H., Riebler, A., Martins, T. G., and Sørbye, S. H. (2017). Penalising model component complexity: A principled, practical approach to constructing priors. *Statistical Science*, 32(1):1–28.

Singh, V., Meena, K. K., and Agarwal, A. (2021). Travellers' exposure to air pollution: A systematic review and future directions. *Urban Climate*, 38:100901.

Smith, R. and Naylor, J. (1987). A comparison of maximum likelihood and Bayesian estimators for the three-parameter Weibull distribution. *Applied Statistics*, 36:358.

Sobolevsky, S. and Campari, R. (2014). General optimization technique for high-quality community detection in complex networks. *Phys. Rev. E*, 90:012811.

Spiegelhalter, D. J., Best, N. G., Carlin, B. P., and van der Linde, A. (2002). Bayesian measures of model complexity and fit. *Journal of the Royal Statistical Society: Series B (Statistical Methodology)*, 64(4):583–639.

Sun, P., Gao, L., and Han, S. (2011). Identification of overlapping and non-overlapping community structure by fuzzy clustering in complex networks. *Inf. Sci.*, 181:1060–1071.

Taheri Shahraiyni, H. and Sodoudi, S. (2016). Statistical modeling approaches for PM₁₀ prediction in urban areas; a review of 21st-Century studies. *Atmosphere*, 7:15.

Tang, Q. and Yuan, Z. (2019). CAT bond pricing under a product probability measure with pot risk characterization. *ASTIN Bulletin*, 49:457 – 490.

Thomas, M., Lemaitre, M., Wilson, M., Viboud, C., Yordanov, Y., Wackernagel, H., and Carrat, F. (2016). Applications of extreme value theory in public health. *PLOS ONE*, 11:e0159312.

Vandeskog, S. M., Martino, S., Castro-Camilo, D., and Rue, H. (2022). Modelling sub-daily precipitation extremes with the blended generalised extreme value distribution. *Journal of Agricultural, Biological and Environmental Statistics*.

Vehlow, C., Reinhardt, T., and Weiskopf, D. (2013). Visualizing fuzzy overlapping communities in networks. *IEEE Trans. Vis. Comput. Graph.*, 19:2486–2495.

Villarini, G. (2016). On the seasonality of flooding across the continental United States. *Advances in Water Resources*, 87:80–91.

Šubelj, L. and Bajec, M. (2011a). Robust network community detection using balanced propagation. *Eur. Phys. J. B.*, 81:353–362.

Šubelj, L. and Bajec, M. (2011b). Unfolding communities in large complex networks: Combining defensive and offensive label propagation for core extraction. *Phys. Rev. E.*, 83:036103.

Šubelj, L. and Bajec, M. (2012). Ubiquitousness of link-density and link-pattern communities in real-world networks. *Eur. Phys. J. B.*, 85:1–11.

Wang, N., Lombardo, L., Tonini, M., Cheng, W., Guo, L., and Xiong, J. (2021). Spatio-temporal clustering of flash floods in a changing climate (China, 1950–2015). *Natural Hazards and Earth System Sciences*, 21:2109–2124.

Wang, W., Liu, D., Liu, X., and Pan, L. (2013). Fuzzy overlapping community detection based on local random walk and multidimensional scaling. *Physica A.*, 392:6578–6586.

Wang, X. and Li, J. (2013). Detecting communities by the core-vertex and intimate degree in complex networks. *Physica A.*, 392:2555–2563.

Watanabe, S. (2013). A widely applicable Bayesian information criterion. *J. Mach. Learn. Res.*, 14(1):867–897.

Wong, F. and Collins, J. J. (2020). Evidence that coronavirus superspreading is fat-tailed. *Proceedings of the National Academy of Sciences*, 117(47):29416–29418.

Yang, X., Zhang, J., and Ren, W.-X. (2018). Threshold selection for extreme value estimation of vehicle load effect on bridges. *International Journal of Distributed Sensor Networks*, 14(2):1550147718757698.

Yu, X., Su, J., Li, X., and Chen, G. (2014). Short-term effects of particulate matter on stroke attack: Meta-regression and meta-analyses. *PloS one*, 9:e95682.

Zhang, S., Wang, R., and Zhang, X. (2007). Identification of overlapping community structure in complex networks using fuzzy c-means clustering. *Physica A.*, 374:483–490.

Zhang, Y. and Yeung, D. (2012). Overlapping community detection via bounded nonnegative matrix tri-factorization. In *In Proc. ACM SIGKDD Conf.*, pages 606–614.

Zheng, L., Ismail, K., Sayed, T., and Fatema, T. (2018). Bivariate extreme value modeling for road safety estimation. *Accident Analysis & Prevention*, 120:83–91.